Naghavi, Saeed; Gao, Jian; Stadius, Kari; Ryynänen, Jussi

A Compact and Wideband mmWave Passive CMOS Circulator Based on Switched All-Pass Networks

Published in:
IEEE Microwave and Wireless Technology Letters

DOI:
10.1109/LMWT.2023.3329963

Published: 01/01/2024

Document Version
Peer-reviewed accepted author manuscript, also known as Final accepted manuscript or Post-print

Please cite the original version:
Naghavi, S., Gao, J., Stadius, K., & Ryynänen, J. (2024). A Compact and Wideband mmWave Passive CMOS Circulator Based on Switched All-Pass Networks. *IEEE Microwave and Wireless Technology Letters*, *34*(1), 41-44. Article 10314534. https://doi.org/10.1109/LMWT.2023.3329963

A Compact and Wideband mmWave Passive CMOS Circulator Based on Switched All-Pass Networks

Saeed Naghavi, Jian Gao, Kari Stadius, Jussi Ryynänen, *Senior Member, IEEE*

***Abstract*—This paper presents a compact and wideband passive CMOS circulator for mmWave phased array transceivers. The paper focuses on achieving a compact die area while still offering competitive performance in terms of loss, isolation, and linearity. Our implemented circulator includes two reciprocal phase shift branches as well as a single-path non-reciprocal phase shift branch. We propose to use first-order lattice all-pass filters with coupled inductors to create the required phase shifts, which offer more compact, wideband, and predictable results compared to conventional lattice all-pass filters with two separate inductors. We also propose to use four identical first-order lattice cells in reciprocal and non-reciprocal branches. This can further reduce the size of the non-reciprocal branch due to fewer inductors compared to a typical second-order all-pass filter like bridged-T. The circuit is implemented in a 28 nm CMOS process, and the active die area is only 0.17 mm^2. Our measurements demonstrate that the implemented circulator operates over a 1 dB insertion loss bandwidth of 14-28 GHz that achieves 66% fractional bandwidth with an insertion loss of 3.8 dB, isolation of over 20 dB, and input third-order intercept point of +19 dBm.**

***Index Terms*—Circulator, CMOS, full-duplex, mmWave, non-magnetic, non-reciprocal, self-interference cancellation.**

I. Introduction

FULL-DUPLEX (FD) mmWave radios are evolving toward higher integration density. At lower microwave frequencies, the size of antennas is still large, making their integration economically unwise. A potential alternative system concept is an external phased antenna array with integrated circulators serving as duplex filters. In such a system, the small die area of the circulator is crucial to enable a cost-effective solution since integrating multiple circulators onto a single die is required. Additionally, while there has been initial progress, existing solutions for integrated circulators at sub-6 GHz do not immediately translate to mmWave systems. Thus, the need for a compact and high-performance integrated circulator operating at mmWave ranges remains an open research challenge.

Initial IC-compatible circulators were proposed using inherent non-reciprocal behavior of active devices [1]–[8]. However, these methods are severely limited by poor noise and linearity performance [9]. Linear periodically time-varying circuits can also be exploited to break the reciprocity [10], [11]. Especially, spatiotemporal modulation of conductivity has shown potential for achieving low noise and highly linear operation [12]–[21]. However, existing solutions are limited by either a large die area or low-frequency operation. N-path filter based circulators [12], for instance, require numerous low-duty-cycle non-overlapping clock signals at the same frequency as the input signal, making it difficult to implement at higher frequencies. Switched transmission line (TL)-based structures [14], on the other hand, use only four 50% duty-cycle I/Q phases and enable switching at a frequency lower than the input signal, which eases mmWave operation. However, the die area is still large due to the use of $\lambda/4$ TLs. Recently, switched all-pass filter based circulator was also examined [17], [18]. This approach achieves a more compact die area by avoiding TLs, yet the number of inductors could still be further reduced. Furthermore, the designed structure operates only at 6.5 GHz and it needs to be scaled up to the mmWave ranges.

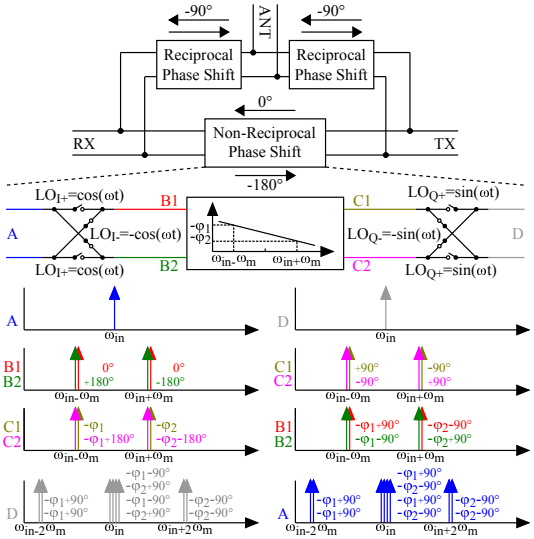

Fig. 1: Phase-frequency domain analysis of the single-path non-reciprocal branch circulator.

In order to address the discussed challenges, this paper presents an integrated circulator that is fabricated on a 28 nm CMOS process. The introduced mmWave circulator aims to achieve a compact die area while still offering competitive performance in terms of loss, isolation, and linearity. In Chapter II we describe the circulator design. Chapter III covers the measurement results, and Chapter IV concludes the paper.

II. Circuit Design and Operation

The circulator is realized using a ring that includes two reciprocal branches with -90° phase shift in either direction and a non-reciprocal branch with 0°/-180° phase shift depending on the signal direction as shown in Fig. 1. The arrangement of phase shifts results in constructive interference in one direction

Manuscript received X XX, 2023; revised X XX, 2023.

S. Naghavi, K. Stadius, and J. Ryynänen are with the Department of Electronics and Nanoengineering, Aalto University, Espoo, Finland (email: saeed.naghavi@aalto.fi).

J. Gao is with the School of Integrated Circuits and Electronics, Beijing Institute of Technology, Beijing 100081, China.

while destructive interference in the opposite direction, which allows signals to propagate only in one direction across the ring. Both reciprocal and non-reciprocal branches create the required phase shifts using passive filters. For this purpose, we have employed all-pass networks, which can offer significant benefits over TL-based structures, including a more compact die area and wider bandwidth [18]. The -90° phase shifts required by reciprocal branches are provided by first-order lattice all-pass filters. The non-reciprocal branch, on the other hand, demands passive filters that are placed between I/Q mixers switched at a frequency lower than the input frequency to facilitate low-power operation. A lower switching frequency corresponds to a longer time delay introduced by the internal filter. When considering a TL-based implementation, as proposed in [15], the corresponding line needs to be extended. This requires more equivalent LC sections ($\frac{\pi}{2} \times \frac{\omega_{in}}{\omega_m}$ sections), resulting in a larger die area to provide the required phase shift, thereby falling into the common tradeoff with loss. However, utilizing a second-order all-pass filter, as suggested in [18], can ideally provide the required phase shift without affecting the amplitude. Furthermore, this approach increases the bandwidth thanks to the highly linear phase response around the center frequency, thus maintaining the required phase relationship over a large frequency band. As the input frequency deviates from the designed center of the all-pass filter, the components $\omega_{in} \pm \omega_m$ move accordingly, and the phase relationship is maintained as long as they both are in the linear region, until one of them falls into the phase plateau regime.

The detailed phase-frequency domain analysis of the non-reciprocal branch is shown in Fig. 1. In the A to D direction, the incoming signal at frequency ω_{in} is first mixed with I clock at frequency ω_m, generating two mixing products at $\omega_{in} \pm \omega_m$. The difference and sum frequency components experience additional phase shifts $-\varphi_1$ and $-\varphi_2$, respectively, caused by the implemented filter. Lastly, the frequency components undergo a second mixing stage with Q clock at frequency ω_m, thus generating mixing products at $\omega_{in} \pm 2\omega_m$. The four mixing products at ω_{in} are in phase and can add up constructively, providing lossless transmission with a $-\varphi_1 - 90^o = -\varphi_2 + 90^o$ phase shift. In the D to A direction, the same analysis shows that a $-\varphi_1 + 90^o = -\varphi_2 - 90^o$ phase shift lossless transmission can be obtained. The resulting S-parameters are:

$$S = \begin{bmatrix} 0 & +e^{j(-\varphi_1+90^o)} \\ +e^{j(-\varphi_1-90^o)} & 0 \end{bmatrix} \quad (1)$$

Thus, the phase-domain conditions for a non-reciprocal operation can be calculated as:

$$\begin{cases} e^{j(-\varphi_1 \pm 90^o)} = \pm 1 \rightarrow \varphi_1 = 90^o \\ -\varphi_1 \mp 90^o = -\varphi_2 \pm 90^o \rightarrow \varphi_2 = 270^o \end{cases} \quad (2)$$

The non-reciprocal branch can be realized using a single- or dual-path configuration, wherein in the dual-path case, an additional quadrature path is placed parallel to the original path. While the dual-path structure is frequently used to minimize the adverse effects of duty cycle mismatch in I/Q clock generation [14], [18], we have utilized a single-path structure to achieve a compact die area. Our simulations show that using a single-path structure, reasonable levels of clock

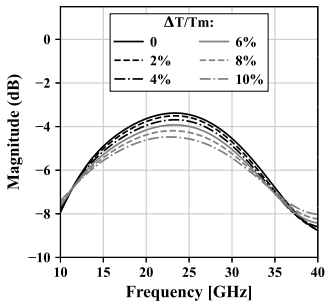

Fig. 2: Simulated circulator loss while considering a deviation from the 50% duty cycle.

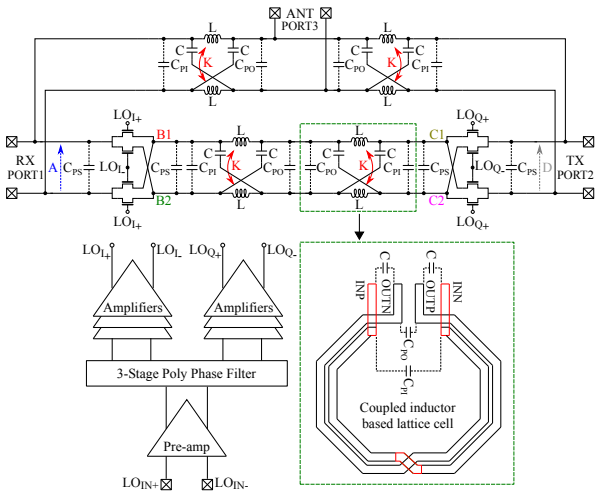

Fig. 3: Proposed circulator. All four LC networks are identical.

impairment still guarantee high-performance characteristics for the circulator. For instance, a 10% deviation from the 50% duty cycle would degrade the overall loss by 1 dB as shown in Fig. 2. Despite this degradation, the circulator loss based on a single-path non-reciprocal branch would still fall within the same range as the dual-path case. This is primarily due to the substantial impact of the ON-resistance (RON) of the switches, contributing to nearly one-third of the circulator loss [14]. By removing the quadrature path, we can effectively double the size of the switches, leading to a 50% reduction in RON while maintaining the same total parasitic capacitance as the dual-path configuration. Additionally, the simulations reveal that the circulator based on a single-path non-reciprocal branch maintains isolation levels over 20 dB and IP1dB over 14 dBm, even when subjected to a duty cycle deviation of up to 10%.

We have further reduced the die area by realizing the required lattice cells with coupled inductors as shown in Fig. 3. It is well-known that utilizing coupled inductors allows for achieving the intended inductance with nearly half the size required by using two separate inductors. In addition to the lattice capacitance itself, the layout of the coupled inductors introduces two parasitic shunt capacitances at the input and output of each lattice cell ($C_{PI} < C_{PO}$), arising from the capacitive coupling between the traces of the inductors. This helps to absorb a significant part of the parasitic capacitances of the switches into the reciprocal and non-reciprocal branches ($C_{PS} + C_{PI} \approx 2C_{PO}$). As a result, the implemented circulator can provide wider bandwidth and improved linearity compared

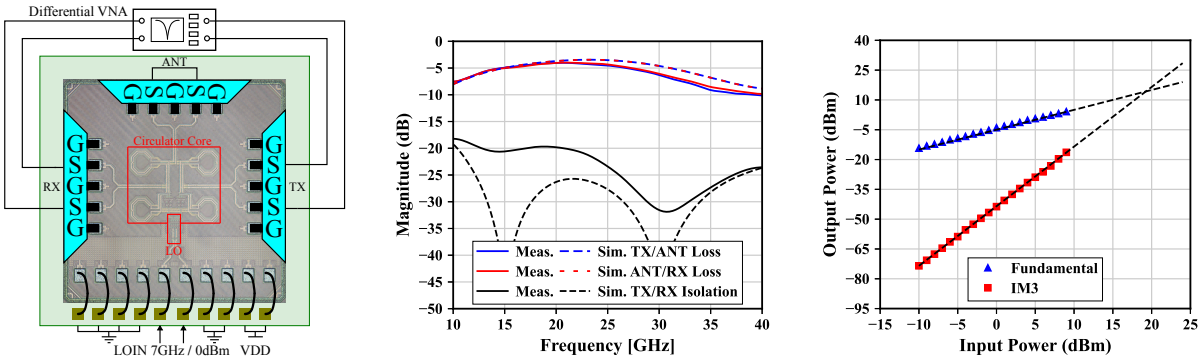

(a) (b) (c)

Fig. 4: Measurement setup and chip photo (a), measured vs simulated loss/isolation (b), measured TX to ANT IIP3 (c).

to the all-pass filter based structure with uncoupled inductors. Additionally, the use of mutually coupled inductors provides more predictable results, as the magnetic fields generated by the currents flowing through the inductors remain confined within the inductor area. Conversely, in the uncoupled case, the fields can spread out in different directions, potentially causing unintended coupling with nearby elements.

We also propose to use four identical first-order cells in reciprocal and non-reciprocal branches as depicted in Fig. 3. Each reciprocal branch employs a first-order cell, and the non-reciprocal branch employs a second-order cell. To form a second-order response, we have used two cascaded first-order cells of the same type as the reciprocal branches. This can further reduce the size of the non-reciprocal branch due to fewer inductors compared to a typical second-order all-pass filter like bridged-T. Also, identical phase shift cells provide more uniform frequency behavior for reciprocal and non-reciprocal branches.

III. Measurement Results

Fig. 4a presents the measurement setup and microphotograph of the chip fabricated on a 28 nm CMOS process. Active die area is only 0.17 mm^2. We chose to operate with a modulation index of 3 ($f_m = f_{in}/3 = 7$ GHz) to prevent a significant decrease in bandwidth while facilitating clock generation, compared to $f_m = 21$ GHz. The power consumption of the circulator is 28.8 mW from a 0.9 V supply voltage. We have used a differential vector network analyzer to measure the S-parameters by probing two differential ports at a time, while a mmWave probe terminated with a broadband termination is landed on the third port. The impedance matching at all ports is always below -10 dB. The measured loss and isolation results after calibration and de-embedding non-circulator losses are depicted in Fig. 4b. The circuit operates over a 1 dB IL bandwidth of 14-28 GHz, thus yielding a 66% fractional bandwidth, with a 3.8 dB IL and over 20 dB isolation. Finally, the circulator's linearity performance has also been measured. The measurement setup limits the measured IP1dB of TX-to-ANT and the result depicts that the circulator does not yet compress at a TX power level of 10 dBm. The measured IIP3, on the other hand, shows the highly linear operation of the proposed circulator with an IIP3 of +19 dBm.

IV. Conclusion

This paper presents a compact and wideband passive CMOS circulator. We proposed (1) to use first-order lattice all-pass filters with coupled inductors to create the required phase shifts, and (2) to use four identical first-order cells in reciprocal and non-reciprocal branches. These techniques offer more compact, wideband, and predictable results. Table I shows the performance summary of the proposed circulator and compares it to the state of the art. The implemented circulator can provide state-of-the-art level characteristics in terms of loss, isolation, and linearity, while it is the most compact and wideband mmWave circulator structure reported.

Acknowledgment

The authors would like to express our gratitude to Mr. Antti Kuhlberg for his contribution to printed circuit board (PCB) fabrication, die attach, and wire-bonding process.

TABLE I: MEASURED PERFORMANCE COMPARISON

	This work	[6] MWCL2014	[7] TMTT2015	[15] TMTT2018	[16] ISSCC2019	[17] RFIC2019	[21] RFIC2022	[22] RFIC2017
Architecture	**Switched Coupled APN**	Active Current-Reuse	Active Power Divider	Switched LPF	Switched BPF	Switched APN	Switched LPF	Parametric NR TL
CMOS Process	**28nm**	180nm	180nm	45nm SOI	45nm SOI	40nm	28nm FDSOI	65nm
1dB BW (GHz)	**14-28**	2.15-2.55	24.17-24.55	22.7-27.3	50-56.8	5.6-7.4	0.05-3.5[1]	92.5-107.5[2]
LO Frequency (GHz)	**7**	N/A	N/A	8.33	8.6	1.3	1.65	10
IL (dB)[3]	**3.8/3.8**	3.7/3.2	5.7/5.7	3.3/3.2	3.6/3.1	2.2/2.2	2.5/2.6	4.5/4.5
Isolation (dB)	**>20**	>25	>20	>18.5	>20	>18	>20	>20
Isolation BW (%)	**66**	16	1.6	18	14.6	28	200	15/1.6[4]
IIP3 (dBm)	**19**	N/A	N/A	20.1/19.9	19.43/19.03	>17.5	N/A	N/A
PWR (mW)	**28.8**	1.5	7.2	78.4	41.04	12.4	20	N/A
Area (mm^2)	**0.17**	0.615	0.715	2.16	1.72	0.45	0.96	0.245

[1] Estimated from the measured results. The reported 2.5dB BW is 0.05-7GHz.
[2] Estimated from the measured results. The reported 2dB BW is 85-110GHz.
[3] TX to ANT / ANT to RX loss.
[4] 20dB isolation BW / 45dB isolation BW.

REFERENCES

[1] S. Tanaka, N. Shimomura, and K. Ohtake, "Active circulators—the realization of circulators using transistors," *Proceedings of the IEEE*, vol. 53, no. 3, pp. 260–267, 1965.

[2] S.-C. Shin, J.-Y. Huang, K.-Y. Lin, and H. Wang, "A 1.5–9.6 GHz monolithic active quasi-circulator in 0.18 μm CMOS technology," *IEEE Microwave and Wireless Components Letters*, vol. 18, no. 12, pp. 797–799, 2008.

[3] C.-H. Chang, Y.-T. Lo, and J.-F. Kiang, "A 30 GHz active quasi-circulator with current-reuse technique in 0.18 μm CMOS technology," *IEEE microwave and wireless components letters*, vol. 20, no. 12, pp. 693–695, 2010.

[4] D.-J. Huang, J.-L. Kuo, and H. Wang, "A 24-GHz low power and high isolation active quasi-circulator," in *2012 IEEE/MTT-S International Microwave Symposium Digest*. IEEE, 2012, pp. 1–3.

[5] S.-H. Hung, K.-W. Cheng, and Y.-H. Wang, "An ultra wideband quasi-circulator with distributed amplifiers using 90 nm CMOS technology," *IEEE microwave and wireless components letters*, vol. 23, no. 12, pp. 656–658, 2013.

[6] J.-Y. Hsieh, T. Wang, and S.-S. Lu, "A 1.5-mW, 2.4 GHz quasi-circulator with high transmitter-to-receiver isolation in CMOS technology," *IEEE Microwave and Wireless Components Letters*, vol. 24, no. 12, pp. 872–874, 2014.

[7] J.-F. Chang, J.-C. Kao, Y.-H. Lin, and H. Wang, "Design and analysis of 24-GHz active isolator and quasi-circulator," *IEEE Transactions on Microwave Theory and Techniques*, vol. 63, no. 8, pp. 2638–2649, 2015.

[8] S. Wang, C.-H. Lee, and Y.-B. Wu, "Fully integrated 10-GHz active circulator and quasi-circulator using bridged-T networks in standard CMOS," *IEEE Transactions on Very Large Scale Integration (VLSI) Systems*, vol. 24, no. 10, pp. 3184–3192, 2016.

[9] G. Carchon and B. Nanwelaers, "Power and noise limitations of active circulators," *IEEE Transactions on Microwave Theory and Techniques*, vol. 48, no. 2, pp. 316–319, 2000.

[10] N. A. Estep, D. L. Sounas, J. Soric, and A. Alu, "Magnetic-free non-reciprocity and isolation based on parametrically modulated coupled-resonator loops," *Nature Physics*, vol. 10, no. 12, pp. 923–927, 2014.

[11] A. Kord, M. Tymchenko, D. L. Sounas, H. Krishnaswamy, and A. Alù, "CMOS integrated magnetless circulators based on spatiotemporal modulation angular-momentum biasing," *IEEE Transactions on Microwave Theory and Techniques*, vol. 67, no. 7, pp. 2649–2662, 2019.

[12] N. Reiskarimian, J. Zhou, and H. Krishnaswamy, "A CMOS passive LPTV nonmagnetic circulator and its application in a full-duplex receiver," *IEEE Journal of Solid-State Circuits*, vol. 52, no. 5, pp. 1358–1372, 2017.

[13] N. Reiskarimian, M. B. Dastjerdi, J. Zhou, and H. Krishnaswamy, "Analysis and design of commutation-based circulator-receivers for integrated full-duplex wireless," *IEEE Journal of Solid-State Circuits*, vol. 53, no. 8, pp. 2190–2201, 2018.

[14] T. Dinc, A. Nagulu, and H. Krishnaswamy, "A millimeter-wave non-magnetic passive SOI CMOS circulator based on spatio-temporal conductivity modulation," *IEEE Journal of Solid-State Circuits*, vol. 52, no. 12, pp. 3276–3292, 2017.

[15] A. Nagulu, T. Dinc, Z. Xiao, M. Tymchenko, D. L. Sounas, A. Alù, and H. Krishnaswamy, "Nonreciprocal components based on switched transmission lines," *IEEE Transactions on Microwave Theory and Techniques*, vol. 66, no. 11, pp. 4706–4725, 2018.

[16] A. Nagulu and H. Krishnaswamy, "28.5 non-magnetic 60GHz SOI CMOS circulator based on loss/dispersion-engineered switched bandpass filters," in *2019 IEEE International Solid-State Circuits Conference-(ISSCC)*. IEEE, 2019, pp. 446–448.

[17] A. Ruffino, Y. Peng, F. Sebastiano, M. Babaie, and E. Charbon, "A 6.5 GHz cryogenic all-pass filter circulator in 40-nm CMOS for quantum computing applications," in *2019 IEEE Radio Frequency Integrated Circuits Symposium (RFIC)*. IEEE, 2019, pp. 107–110.

[18] A. Ruffino, Y. Peng, F. Sebastiano, M. Babaie, and E. Charbon, "A wide-band low-power cryogenic CMOS circulator for quantum applications," *IEEE Journal of Solid-State Circuits*, vol. 55, no. 5, pp. 1224–1238, 2020.

[19] M. M. Biedka, R. Zhu, Q. M. Xu, and Y. E. Wang, "Ultra-wide band non-reciprocity through sequentially-switched delay lines," *Scientific reports*, vol. 7, no. 1, pp. 1–16, 2017.

[20] M. Biedka, P. Rodgers, N. Gutierrez, T. LaRocca, and Y. E. Wang, "100MHz to 1GHz on-chip circulator with integrated driver amplifiers," in *2019 IEEE MTT-S International Microwave Symposium (IMS)*. IEEE, 2019, pp. 1488–1491.

[21] J. Hwang and B.-W. Min, "Fully integrated ultra-wideband differential circulator based on sequentially switched delay line in 28-nm FDSOI CMOS," in *2022 IEEE Radio Frequency Integrated Circuits Symposium (RFIC)*. IEEE, 2022, pp. 267–270.

[22] C. Yang and P. Gui, "85–110 GHz CMOS tunable nonreciprocal transmission line with 45 dB isolation for wideband transceivers," in *2017 IEEE Radio Frequency Integrated Circuits Symposium (RFIC)*. IEEE, 2017, pp. 284–287.